NOTES AND CORRESPONDENCE

An Easy Method for Estimation of Q-Vectors from Weather Maps

FREDERICK SANDERS
Marblehead, Massachusetts

BRIAN J. HOSKINS
Department of Meteorology, University of Reading, Reading, United Kingdom

24 July 1989 and 4 December 1989

ABSTRACT

It is shown how to estimate the directions and relative magnitudes of Q-vectors from a map of isobars and isotherms. The divergence of this vector field represents the forcing function in the quasi-geostrophic omega-equation. The direction of the Q-vector at a point is determined by the rate of change of the geostrophic wind vector taken along the isotherms, with the colder air to the left in the Northern Hemisphere. Its direction is 90° to the right of this vector change of wind. The strength of the Q-vector is proportional to the magnitude of the rate of vector wind change, and to the magnitude of the temperature gradient.

Application to an actual situation is shown and compared with the traditional inferences from advections of temperature and vorticity. General agreement is found. Patterns of Q-vectors and associated vertical motion are sketched for idealized patterns of surface lows and highs and for upper-level troughs and ridges. Examples of confluent frontogenesis are shown, for a lower-tropospheric col and for a upper-level jet entrance. Patterns of Q-vectors and vertical circulations are noted for frontogenetical and frontolytical situations.

1. Introduction

Quasi-geostrophic theory has provided the conceptual basis for understanding the behavior of extratropical synoptic systems for more than 30 years. Perhaps its most widely used expression is the omega equation, for diagnosing vertical motion from fields of geopotential height and temperature, as discussed in detail by Durran and Snellman (1987). The traditional form of this equation, following these authors, is

$$\left(\sigma\nabla^2 + f_0^2\frac{\partial^2}{\partial p^2}\right)\omega = f_0\frac{\partial}{\partial p}\left[\mathbf{V}_g\cdot\nabla\left(\frac{1}{f_0}\nabla^2\Phi + f\right)\right] + \nabla^2\left[\mathbf{V}_g\cdot\nabla\left(-\frac{\partial\Phi}{\partial p}\right)\right], \quad (1)$$

where $\omega = dp/dt$ represents the vertical motion, the subscript g denotes the geostrophic value, f is the coriolis parameter, σ a stability factor and Φ the geopotential, gz. The two terms on the right-hand side represent the effects of vorticity advection and temperature advection.

Even with systems possessing simple vertical structure, in contrast to the one cited by Durran and Snellman (1987), an undesirable feature of this traditional way of looking at the right-hand side of (1) is that the two terms often tend to cancel. This note is intended to provide an improved method of qualitative interpretation based on the Q-vector approach of Hoskins et al. (1978).

Given the substantial volume of quantitative guidance products produced by the National Meteorological Center (NMC) and other major centralized facilities, and given the anticipated increase in ability to perform calculations at local forecast offices, the question arises whether qualitative interpretation is of operational interest. At present it is useful in a number of circumstances.

First, some pressure and temperature fields are available without accompanying diagnoses of vertical motion. These might be sectional surface analyses based on the latest round of hourly observations in a rapidly developing situation. Alternatively, they might be model prognoses for which the basic pressure and temperature fields are available, but communication limitations make it impossible to transmit accompanying fields of vertical motion, humidity, and precipitation, even though they are part of the forecast calculation. This is the current situation for the medium-range forecast run of NMC's global spectral model. Indeed, the initial analysis in any of NMC's models lacks a representation of vertical motion. In either of these circumstances it is useful to be able to infer from the available maps something about the fields of vertical motion, cloud, and precipitation.

Second, even when prognostic vertical motions are

Corresponding author address: Frederick Sanders, 9 Flint Street, Marblehead, MA 01945.

available to the forecaster, as in the nested grid model (NGM), suspicious features may show up from time to time. In assessing credibility, the forecaster may wish to look qualitatively at the pressure and temperature fields to see whether the ascent or descent in question looks reasonable.

In either of these types of circumstances, quasi-geostrophic diagnosis may not be as accurate as a more sophisticated calculation, but it is decidedly useful. It is hard to imagine that these cases will not happen in the foreseeable future.

The future, moreover, will surely continue the increasing availability of numerical predictions from a number of forecast centers. A third, and perhaps more profound use for quasi-geostrophic diagnosis will then be to give a sophisticated comparison of these predictions with each other as well as with observations of various types received subsequent to the initial time of the forecasts.

2. An illustrative example

Consider as an example (in which we already know the answer) the situation shown in Fig. 1, a 12-h forecast produced by the nested grid model (NGM). Associated with the surface cyclone centered near 40°N, 90°W, there is a region of maximum warm advection around 41°N, 81°W and a region of maximum cold advection around 36°N, 97°W. At 500 mb the intense vorticity maximum near 37°N, 93°W is associated with strong cyclonic advection to its east and anticyclonic advection to its west.

Careful comparison of Figs. 1(a) and (b) shows that part of the region of cold advection south of the low center, tending to force descent, is a region of cyclonic vorticity advection aloft, tending to force ascent at tropospheric levels below. Other examples of opposing effects are seen in the easternmost part of the region of warm advection around 40°N, 78°W, where weak anticyclonic vorticity advection for the most part is occurring aloft, and in the vicinity of 43°N, 102°W, where cold advection is accompanied by cyclonic vorticity advection. Interpretation of the net effect in these regions by the traditional method is not clear. The NGM vertical-motion pattern in Fig. 1(c) shows that vorticity advection dominates in the first of these regions of opposing effects and that the net effect is small in the other two.

Maxima and minima of vertical motion occur in regions where one or the other of the effects is large and the other is supportive or slight. Nevertheless, in the structure of simple baroclinic waves, with the upper trough (ridge) lagging (usually westward) behind the surface low (high), it is inevitable that the easternmost portions of the temperature advection areas are characterized by upper-level vorticity advections in the opposing sense so far as vertical motion is concerned. Here the interpretation of the situation by traditional methods will always be difficult.

3. Q-vectors

Hoskins et al. (1978) showed that the right-hand side of the omega equation—neglecting the small effect due to the variation of the Coriolis parameter with latitude—could be written in a way that avoids this potential cancellation effect; i.e.,

$$\left(\sigma\nabla^2 + f_0^2\frac{\partial^2}{\partial p^2}\right)\omega = -2\nabla\cdot\mathbf{Q}. \qquad (2)$$

This compact form of the equation shows that the vertical motion tends to be upward when the field of **Q**-vectors is convergent. The vector itself indicates the horizontal gradient of vertical motion and the vertical gradient of the ageostrophic wind component, as required to maintain hydrostatic- and thermal-wind balance in the face of the disruptive advections of temperature and vorticity. If the synoptic system is sufficiently deep to fill the entire troposphere, then the **Q**-vector indicates the direction of the lower-tropospheric ageostrophic motion and points toward the region of ascent. In the high troposphere the direction of the ageostrophic motion is opposite to the **Q**-vector.

A number of studies in the last few years have employed this approach (e.g., Barnes 1985; Bluestein et al. 1988; Branick et al. 1988; O'Handley and Bosart 1989). On the other hand, it has found little operational application despite its simplicity and theoretical advantage. Even in research, although the **Q**-vector expression may be the basis of computation, the interpretation is sometimes (e.g., Branick et al. 1988) in terms of temperature and vorticity advections.

The reason for this limitation might be a difficulty in assessing the **Q**-vector by inspection of charts. After all, nothing is easier than determining the sense and relative magnitude of a geostrophic advection by noting the density of points of intersection of height contours and isopleths of temperature or vorticity. Hoskins et al. (1978) pointed out that **Q** is the vector rate of change of temperature gradient following a hypothetical geostrophic (isobaric) trajectory, but this fact has not led to a convenient way of assessing its direction and relative magnitude.

4. Interpretation of Q-vectors

The problem may be the apparent complexity of the expression for **Q**

$$\mathbf{Q} \equiv \left[\frac{\partial \mathbf{V}_g}{\partial x}\cdot\nabla\left(\frac{\partial\Phi}{\partial p}\right),\ \frac{\partial \mathbf{V}_g}{\partial y}\cdot\nabla\left(\frac{\partial\Phi}{\partial p}\right)\right], \qquad (3)$$

where the expressions separated by a comma on the right-hand side are the components in the x- and y-directions. Note that

$$\left.\begin{aligned}\frac{\partial \mathbf{V}_g}{\partial x} &= \frac{\partial u_g}{\partial x}\,\mathbf{i} + \frac{\partial v_g}{\partial x}\,\mathbf{j}\\ \frac{\partial \mathbf{V}_g}{\partial y} &= \frac{\partial u_g}{\partial y}\,\mathbf{i} + \frac{\partial v_g}{\partial y}\,\mathbf{j}\end{aligned}\right\},$$

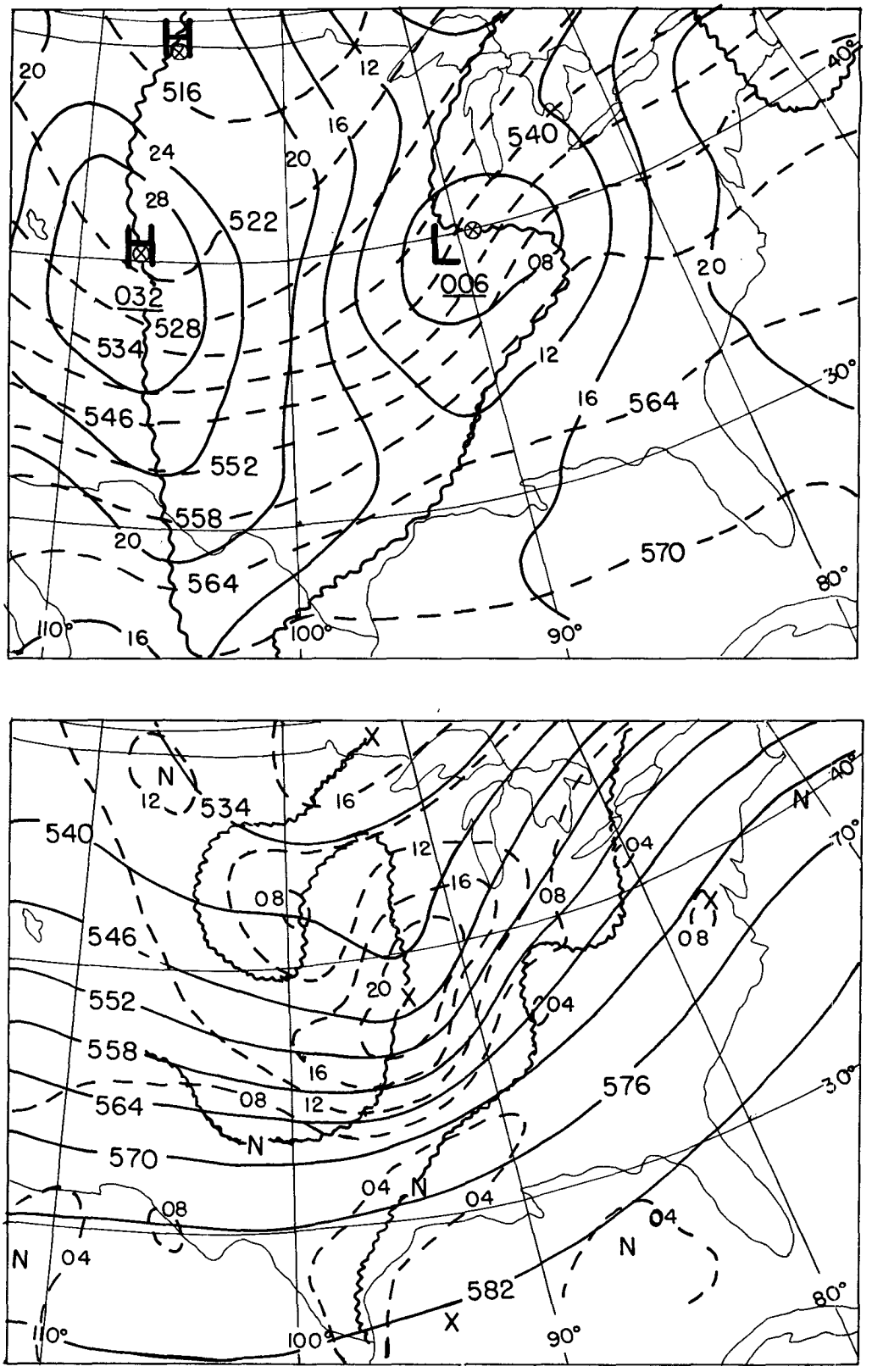

FIG. 1. A 12-h forecast from the nested grid model, verifying at 1200 UTC 24 December 1988: (a) Sea-level isobars at intervals of 4 mb (solid) and thickness lines for the layer from 1000 to 500 mb at intervals of 6 dam (dashed). Heavy wavy lines show selected boundaries of regions of warm and cold advection. (b) Contours of 500-mb height at intervals of 6 dam (solid) and isopleths of absolute vorticity at intervals of 4×10^{-5} s^{-1}. Heavy wavy lines show selected boundaries of regions of cyclonic and anticyclonic vorticity advection. (c) Isopleths of 700-mb omega, with sign reversed, in units of 10^{-3} mb s^{-1}.

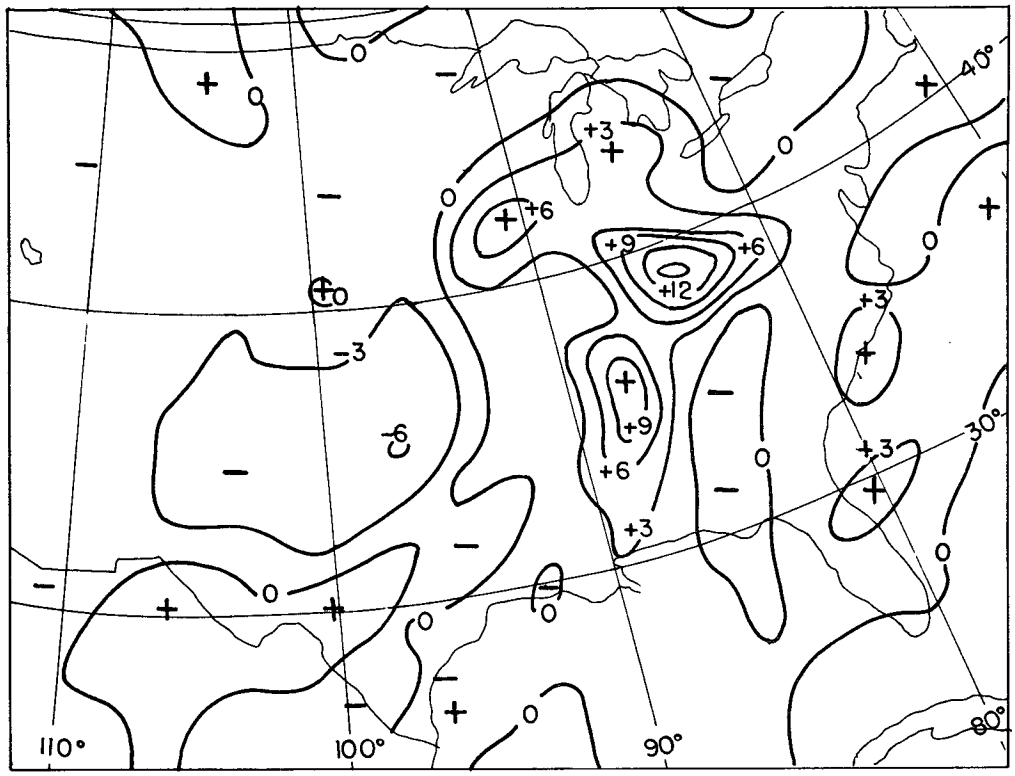

FIG. 1. (*Continued*)

where **i** and **j** are the unit vectors along the x- and y-axes. Note further that, hydrostatically,

$$\nabla\left(\frac{\partial\Phi}{\partial p}\right) = -\frac{R}{p}\nabla T.$$

In fact, Hoskins (1982) mentioned, and Thorpe (1985) applied a convenient way of visualizing **Q**-vectors. Keyser et al. (1988) have also pointed this out, but without elaboration or application.

To derive the appropriate expression, note that the x- and y-axes are mutually orthogonal but are subject to no other restriction. Take the x-axis along the isotherm at a given point. Then

$$\nabla\left(\frac{\partial\Phi}{\partial p}\right) = -\frac{R}{p}\left(\frac{\partial T}{\partial y}\right)\mathbf{j},$$

and (3) becomes

$$\mathbf{Q} = -\frac{R}{p}\left(\frac{\partial T}{\partial y}\right)\left(\frac{\partial v_g}{\partial x}\mathbf{i} + \frac{\partial v_g}{\partial y}\mathbf{j}\right).$$

Now, since with a constant value of f, the divergence of the geostrophic wind is zero, it follows that

$$\frac{\partial v_g}{\partial y} = -\frac{\partial u_g}{\partial x}.$$

We can write

$$\mathbf{Q} = -\frac{R}{p}\left(\frac{\partial T}{\partial y}\right)\left(\frac{\partial v_g}{\partial x}\mathbf{i} - \frac{\partial u_g}{\partial x}\mathbf{j}\right)$$

or, using a vector identity,

$$\mathbf{Q} = -\frac{R}{p}\left|\frac{\partial T}{\partial y}\right|\mathbf{k}\times\frac{\partial \mathbf{V}_g}{\partial x} \qquad (4)$$

where **k** is the unit vertical vector. According to this expression the **Q**-vector can be obtained by traveling along the isotherm with the cold air to the left and noting the *vector* change of the geostrophic wind. Rotation of this vector change 90° clockwise gives the direction of the **Q**-vector. Its magnitude is proportional to the magnitude of the vector rate of change multiplied by the strength of the temperature gradient.

5. Application

This result can be applied qualitatively to the situation shown in Fig. 1(a), assuming that the lower-tropospheric isotherms resemble the thickness lines to obtain the **Q**-vectors near the surface. First, look in Fig. 2 along the channel between the 540- and 546-dam thickness lines. This channel is in the heart of the strongest temperature gradient and coincides with

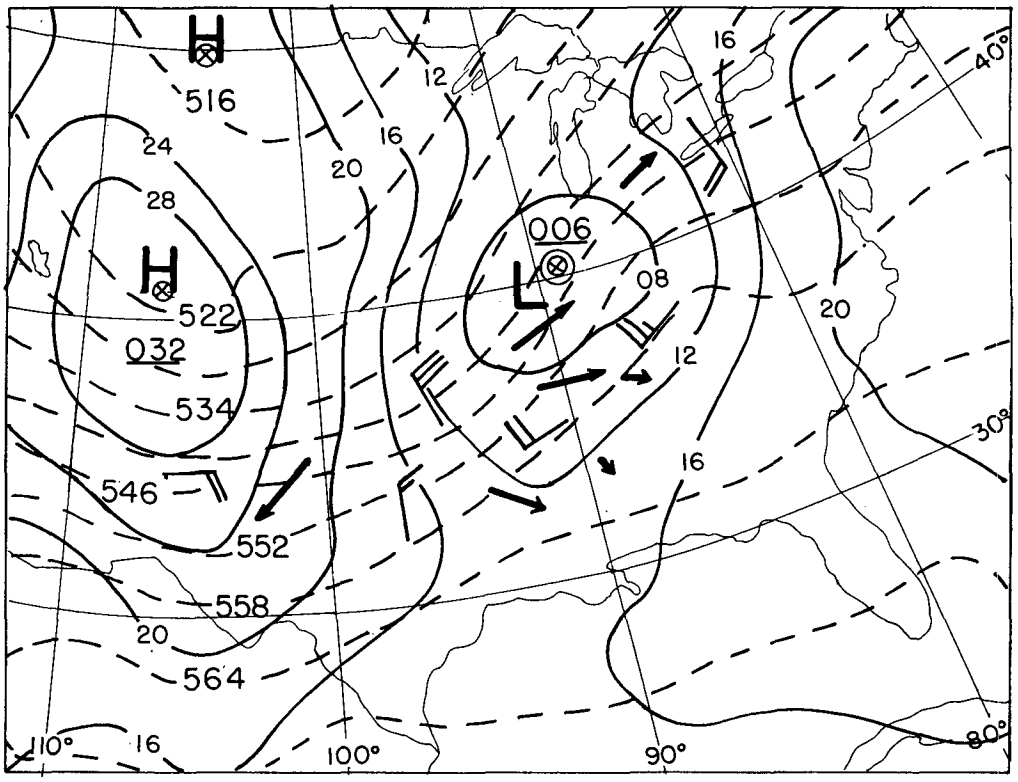

FIG. 2. As in Fig. 1 (a), but with selected geostrophic winds (conventional notation) and Q-vectors (bold arrows) added. The magnitude of the Q-vector is indicated qualitatively by the length of the arrow. See text.

strong and varying geostrophic winds. Therefore it is expected to yield large Q-vectors which will likely dominate the divergence picture. We could evaluate the wind at closely spaced points along this channel and normal to it, so that the directions of the thickness lines at the midpoints would closely approximate the directions of the x- and y-axes required by equation (4). For economy of effort, we will use only a few points, widely spaced, with the orientation of the thickness lines at the midpoints indicating approximately the correct directions.

At the isobaric ridge near 35°N, 107°W, the geostrophic wind in the channel is E at about 20 kt. Down the channel, near 36°N, 96°W, the wind is NNW about 30 kt, so the vector change is NW and the Q-vector is NE between these points. The magnitude is substantial because both the rate of wind change and the temperature gradient are large. Proceeding down the channel from this point to the low center, where the geostrophic wind is zero by definition, the wind change is SSE so the Q-vector is WSW in-between, and likewise of substantial magnitude. Notice that the two Q-vectors thus estimated along the x-direction contribute strongly to divergence around 36°N, 96°W, indicating the descent shown in this region in Fig. 1(c). Some further estimation will show that the variation of the Q-vectors in the y-direction contributes only slightly to the divergence.

Continuing down the channel from the low center, another similar distance brings us to 43°N, 81°W, where the wind is SSE about 20 kt. The change over the distance from the low is of course SSE, so that the Q-vector is again WSW. But it is not as strong as in the preceding estimate west of the low center, because the wind change is not as great, nor is the temperature gradient quite as strong. So these last two Q-vectors indicate convergence over the low center. Indeed, the NGM predicted the low to deepen 8 mb in the next 12 h. From this example, a diffluent thermal wind field over the low, with stronger geostrophic wind behind the low than ahead, appears to be a structure favoring intensification of a surface cyclone.

South of the low center, say, near 35°N, 90°W, where it was noted that the traditional method is somewhat ambiguous, the Q-vectors can be assessed along the 558-dam thickness line. To the southwest, the geostrophic wind is N about 15 kt, while near 35°N, 90°W and to the northeast it is uniformly WSW with a slight downstream increase in speed. The temperature gradient is stronger to the southwest than to the northeast. The Q-vectors are then WNW of moderate strength upstream in the thermal wind, becoming slight downstream. Looking normal to the 558-line, we estimate the Q-vectors to be strong westerly in the colder air and weak in the warmer air. Low-level convergence is indicated, consistent with the ascent seen in Fig. 1(c).

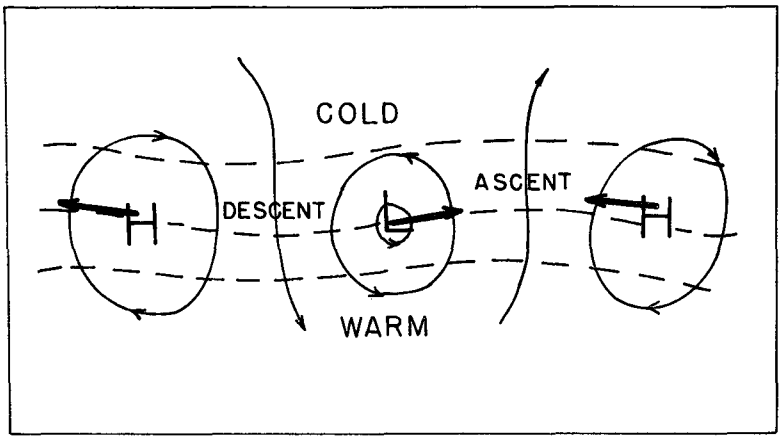

FIG. 3. Idealized pattern of sea-level isobars (solid) and isotherms (dashed) for a train of cyclones and anticyclones. Heavy bold arrows are Q-vectors.

To be certain of the quasi-geostrophic vertical motion, of course, we would have to calculate an adequately complete field of the forcing function (Q-vectors in this case) and solve the omega equation. Details on how to do this are provided by Durran and Snellman (1987), and it may be possible to perform such calculations at a forecast office. Computing the Q-vectors without proceding to solve the omega-equation would be useful, even if it were carried out only over the local area. The aim here, however, is quick estimation, not calculation. The reader is invited to explore Fig. 2, estimating additional Q-vectors, and comparing their regions of obvious convergence and divergence with the pattern of vertical motion seen in Fig. 1(c).

It is useful to look at some idealized examples, to assure that the Q-vector method yields results which are consistent with traditional quasi-geostrophic interpretation and with common experience. A surface low flanked by highs upstream and downstream in a westerly thermal wind field, only slightly perturbed, is shown in Fig. 3. Over the low, the Q-vector is along the thermal wind, because the geostrophic wind change is from northerly behind the low to southerly ahead. Over the highs, the Q-vector is against the thermal wind because the change of wind is from northerly ahead to southerly behind. Hence, low-level convergence and ascent is indicated between the low and the downstream high, while divergence and subsidence is implied between the high and the downstream low. This is consistent with experience and with the association between temperature advection and vertical motion.

The upper-trough and -ridge pattern appearing in Fig. 4 shows no temperature advection, because the isotherms and height contours are mutually parallel.

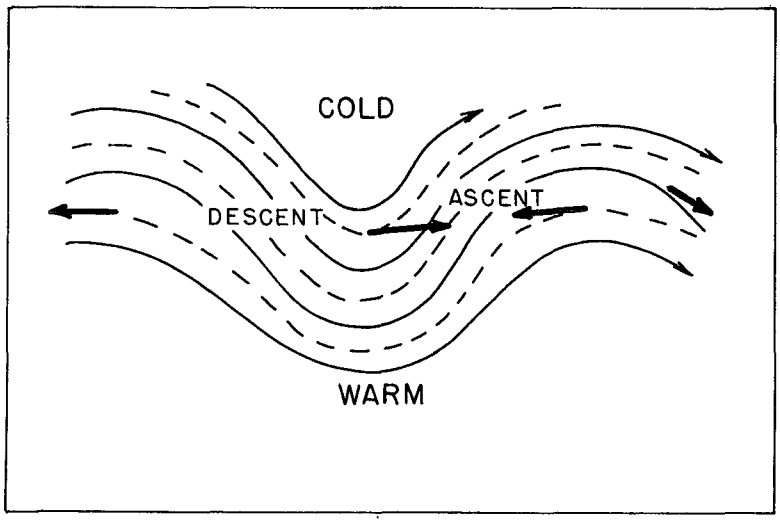

FIG. 4. Idealized pattern of upper-level geopotential height contours (solid) and isotherms (dashed) for a train of equivalent-barotropic troughs and ridges. Heavy bold arrows are Q-vectors.

Across the trough line, however, the Q-vector is westerly because the wind changes from NW to SW along the curving isotherm. Across the ridge line, the corresponding wind changes are reversed and the Q-vector is easterly. Therefore, ascent (descent) is implied downstream from the trough (ridge), consistent with reasoning based on vorticity advection.

An idealized pattern of confluent frontogenesis, corresponding to an upper-level jet-entrance region, is illustrated in Fig. 5. The Q-vectors at both lower or upper levels point directly across the isotherms toward warmer air, in which ascent is implied while the colder air descends. This result is consistent with tradition notions of the relative vertical motions of the air masses at a front.

An important insight in all this is that the frontogenetical forcing, rather than the existence of a front, accounts for the frontal patterns of vertical motion and weather. Different portions of the same baroclinic zone can have different patterns of frontogenetical (or frontolytical) forcing. In Fig. 6, for example, the left-hand portion shows the same orientation of isotherms and Q-vectors as indicated in Fig. 5(a), which may well result in the development of an intense surface front. On the other hand, the right-hand portion shows the opposite, as would be the case if the positions of the highs and lows in Fig. 5(a) were exchanged. The Q-vectors now point toward colder air. Frontolysis is indicated by the pattern of geostrophic advection and descent in the warm air. Ascent in the colder air would likely be weak because of the lower moisture amount and larger effective stability there. In-between, there would be a place where the Q-vectors and isotherms are parallel. Here the baroclinic zone is inactive and

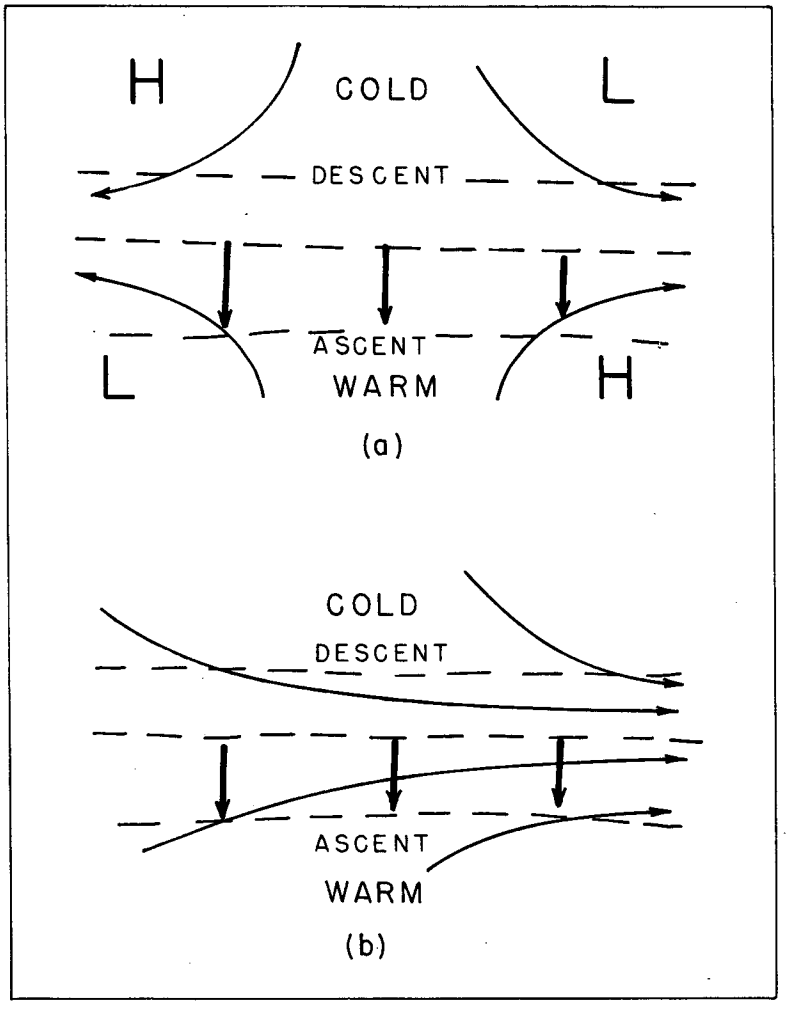

FIG. 5. Idealized confluent frontogenetical patterns. In (a) the solid lines are sea-level isobars and the dashed lines are isotherms. In (b) the isobars in panel a are reinterpreted as contours of low-level geopotential height and the isotherms reinterpreted as isopleths of thickness from the lower-elevation pressure level to some pressure level at a higher elevation. Graphical addition yields a flow pattern representing a jet-entrance region. Heavy bold arrows are Q-vectors.

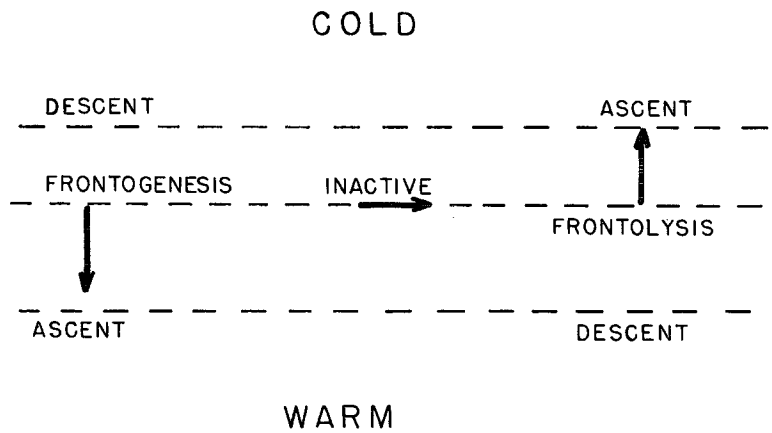

FIG. 6. An idealized baroclinic zone showing regions of frontogenesis, inaction, and frontolysis. The dashed lines are isotherms and the heavy bold arrows are **Q**-vectors.

vertical motions would be weak. Keyser et al. (1988) have provided a detailed explanation of the relationship of **Q**-vectors to frontogenesis. They take into account the influences on both the magnitude of the temperature gradient, as in the above example, and on its direction. These concepts are confirmed in more sophisticated formulations, such as the semi-geostrophic model.

6. Concluding remarks

From any expression of quasi-geostrophic theory we can hope to obtain the broad aspects of the vertical-motion pattern, but not the details. Note in Fig. 1(c) that there are three small but intense centers embedded within the region of general ascent associated with the synoptic system. These are each associated with maxima of precipitation, so it is likely that localized latent-heat release, rather than forcing on a scale likely to be revealed by **Q**-vector divergence (or another form of the forcing in the omega-equation), is responsible for them. Other small wiggles and centers in the pattern of vertical motion are also likely to escape detection in a quasi-geostrophic diagnosis.

Our intent here is to encourage use of the **Q**-vector approach in quasi-geostrophic diagnosis of analyzed or prognostic weather situations by providing a convenient method of quick and qualitative assessment. In general, the results derived from this technique may closely resemble those from the technique suggested by Trenberth (1978), which is consistent with the Sutcliffe (1947) approximation. In this technique, the advection of the vorticity in the middle of a layer by the thermal wind over its depth represents the quasi-geostrophic forcing of omega. In frontogenetical situations, however, the **Q**-vector approach may be more accurate. We hope that the method put forth here will enable operational meteorologists to take advantage of the accuracy and unambiguous character of the **Q**-vector approach. Potential applications include situations where vertical motions calculated from model diagnoses or prognoses are not available, or when display features appear to be questionable. We hope **Q**-vector diagnosis will facilitate comparison of model forecasts with each other and with later data. As models become more complex, the array of diagnostic procedures available to the forecaster must become more sophisticated, or the forecaster will become someone who merely dresses the numerical product in words.

Acknowledgments. We are grateful to the Center for Meteorology and Physical Oceanography, Massachusetts Institute of Technology, for provision of data and facilities, and to Isabelle Kole for the drafting of figures. The work was supported in part by the National Science Foundation Grant ATM-8804110.

REFERENCES

Barnes, S. L. 1985. Omega diagnostics as a supplement to LFM/MOS guidance in weakly forced convective situations. *Mon. Wea. Rev.*, **113:** 2122–2141.

Bluestein, H. C. B., E. W. McCaul, Jr., G. P. Byrd and G. R. Woodall. 1988. Mobile sounding observations of a tornadic storm near the dryline: The Canadian, Texas, storm of 7 May 1986. *Mon. Wea. Rev.* **116:** 1790–1804.

Branick, M. L., F. Vitale, C.-C. Lai and L. F. Bosart. 1988. The synoptic and subsynoptic structure of a long-lived convective storm. *Mon. Wea. Rev.* **116:** 1335–1370.

Durran, D. R., and L. W. Snellman. 1987. The diagnosis of synoptic-scale vertical motion in an operational environment. *Wea. Forecasting* **2:** 17–31.

Hoskins, B. J. 1982. The mathematical theory of frontogenesis. *Ann. Rev. Fluid Mech.* **14:** 131–151.

——, I. Draghici and H. C. Davies. 1978. A new look at the omega-equation. *Quart. J. Roy. Met. Soc.* **104:** 31–38.

Keyser, D., M. J. Reeder and R. J. Reed. 1988. A generalization of Petterssen's frontogenesis function and its relation to the forcing of vertical motion. *Mon. Wea. Rev.* **116:** 762–780.

O'Handley, C., and L. F. Bosart. 1989. Subsynoptic-scale structure in a major synoptic-scale cyclone. *Mon. Wea. Rev.* **117:** 607–630.

Sutcliffe, R. C. 1947. A contribution to the problem of development. *Quart. J. Roy. Meteor. Soc.* **73:** 370–383.

Thorpe, A. 1985. The cold front of 13 January 1983. *Weather* **40:** 34–42.

Trenberth, K. E. 1978. On the interpretation of the diagnostic quasi-geostrophic omega equation. *Mon. Wea. Rev.* **106:** 131–137.